ELSEVIER

Deep-Sea Research II 52 (2005) 1133–1155

DEEP-SEA RESEARCH
PART II

www.elsevier.com/locate/dsr2

Measurement and simulation of viscous dissipation in the wave affected surface layer

Adolf Stips[a,*], Hans Burchard[b], Karsten Bolding[c], Hartmut Prandke[d], André Simon[e], Alfred Wüest[f]

[a]*CEC Joint Research Centre, Institute for Environment and Sustainability, I-21020 Ispra(VA), Italy*
[b]*Institute for Baltic Sea Research, Universität Rostock, Seestrasse 15, D-18119 Rostock, Germany*
[c]*Bolding & Burchard Hydrodynamics GbR, Strandgyden 25, DK 5466 Asperup, Denmark*
[d]*ISW Wassermesstechnik Dr. Hartmut Prandke, Lenzer Street 5, D-17213 Petersdorf, Germany*
[e]*EAWAG, CH-8600 Dübendorf, Switzerland*
[f]*Applied Aquatic Ecology, EAWAG, CH-6047 Kastanienbaum, Switzerland*

Accepted 15 January 2005

Abstract

In this study we compare turbulence parameters from field observations and model simulations specifically under the influence of weak to moderate wind forcing and breaking short waves. The experiment was performed during 12 days under very weak stratification at a fetch-limited lake in Switzerland. The near surface observations were obtained by using a quasi-free rising profiler which measured small scale shear and temperature fluctuations. We used a two-equation k–ε turbulence model with an algebraic second-moment closure scheme. The one-dimensional numerical model was extended to consider breaking waves by a shear-dependent parameterisation.

The agreement of observed and simulated turbulence quantities is very promising. Especially well simulated is the enhanced turbulence level in the wave-affected-surface-layer (WASL) of a few dm thickness. The logarithmic slope of the turbulent dissipation rate in this WASL was found to vary between -2.1 and -1.7. Below the WASL the classic *law-of-the-wall* was well reproduced by the data and the model.

1. Introduction

The surface boundary layer (SBL) of natural waters is a corner stone of earth sciences. Understanding and adequate parameterisation of heat, gas and momentum exchange with the atmosphere—especially under breaking waves—is fundamental for the physical and biogeochemical processes in oceans, lakes and reservoirs.

The early measurements in lakes (Thorpe, 1977; Dillon et al., 1981) and oceans (Lombardo and Gregg, 1989) revealed regularly logarithmic velocity profiles with rates of dissipation ε of turbulent

*Corresponding author.
E-mail address: adolf.stips@jrc.it (Adolf Stips).

0967-0645/$ - see front matter © 2005 Elsevier Ltd. All rights reserved.
doi:10.1016/j.dsr2.2005.01.012

kinetic energy (TKE) increasing proportional to the inverse of depth. Subsequently, the first adopted SBL turbulence model was the concept of the *law-of-the-wall* (LOW), which is a special case of the Monin-Obukhov theory (Monin and Obukhov, 1954; Businger et al., 1971) for zero vertical buoyancy flux.

As experimental techniques improved and turbulence could be measured with better spatial and temporal resolution a more realistic and consistent picture of the top 1 m of the SBL emerged. In the uppermost layer, Kitaigorodskii et al. (1983) found turbulence levels to depend on the surface wave energy with dissipation rates being one or two orders of magnitude above those predicted by LOW. It was shown extensively in Lake Ontario that this extra turbulence is injected by breaking waves (Agrawal et al., 1992; Terray et al., 1996; Drennan et al., 1996; Donelan, 1998). Measurements in the ocean by upward-operated microstructure profilers (Soloviev et al., 1988; Anis and Moum, 1992,1995; Lass and Prandke, 2003), profiling surface buoys by Gemmrich and Farmer (1999) and by horizontally manoeuvred vessels or submarines (Soloviev and Lukas, 2003; Greenan et al., 2001; Osborn et al., 1992; Thorpe et al., 2003) strengthened the view that within several significant wave heights (typically < 2 m) the dissipation rate is at least an order of magnitude above LOW levels. Dissipation was found specifically concentrated in bubble clouds (Thorpe et al., 2003). This so-called wave-affected-surface-layer (WASL) was found to consist of a two-layer structure (Terray et al., 1996). According to their model, approximately half of the TKE dissipation occurs in the very top, so-called wave-turbulent sublayer (Benilov and Ly, 2002), where TKE injection by wave breaking dominates, production by shear is comparably negligible and ε is approximately constant. Below this depth, there is a transition-turbulent sublayer, where the vertical diffusion of TKE still exceeds the local shear production. In this sublayer dissipation rates scale with wind-wave parameters and the depth dependence of ε has logarithmic slopes of -2.3 ± 0.4, depending on the wave height and the wave age. Below, the transition-turbulent sublayer merges with the LOW layer, where turbulence production and dissipation are in balance.

SBL modelling is thus challenged by this complexity of the SBL structure (Zhang and Chan, 2003). Craig and Banner (1994) and Craig (1996) employed an improved level-2.5 closure model to reproduce the observed SBL turbulence. The effect of wave breaking was modelled by a TKE flux into the surface. By prescribing the macro (integral) length scale from LOW scaling, they presented an analytical solution which combines the WASL on top of the LOW including the transition zone in between those two layers. Recently, Burchard (2001a) incorporated those ideas in an extended k–ε turbulence model, allowing to simulate the dynamics in the WASL on top of the logarithmic layer, which is adequately reproduced by unmodified k–ε models.

Since it is empirically not proven that the macro length scales the same way in the WASL and under LOW conditions, Umlauf and Burchard (2003) developed a generic two-equation model which allows for different length scale slopes in both regimes. This was motivated by observations in grid-generated, shear-free turbulence, where the length scale had slopes of $L = 0.2$ rather than the von Kàrmàn parameter of $\kappa = 0.41$ as under LOW conditions. Recently, Kantha and Clayson (2004) extended the k–kl model by Mellor and Yamada (1982) such that the effects of surface wave breaking on near-surface turbulence is reproduced by that model as well. Their model predicts a length scale slope ratio of $\kappa/L = 1.8$, a value which is close to some laboratory data from grid stirring experiments. However, due to the uncertainty of whether grid stirring experiments are a good approximation for surface wave breaking, we use here the model by Burchard (2001a) with $\kappa = L = 0.41$.

Apart from the near-surface length scale slope, two other model parameterisations for surface wave breaking are in the current scientific debate: the height of the unresolved wave-turbulent sublayer, z_0, and the surface flux of TKE, $F_s(k)$. For the latter, usually $F_s(k) \propto |u_*|^3$ (with the surface friction velocity u_*) is used, where the parameter of proportionality may depend on wave age (Terray et al., 1996, 1999). However, often a

constant parameter of proportionality is chosen, as in e.g. Craig and Banner (1994). This choice of the surface TKE flux originally introduced by Craig and Banner (1994) is not in agreement with the physically correct definition $F_s = \overline{c_p} u_*^2$ (with $\overline{c_p}$ is the effective phase speed of waves acquiring energy from the wind) which is for instance given by Gemmrich et al. (1994) and Phillips et al. (2001). For practical applications the difference between these formulations might be small, and is determined by the choice of the corresponding proportionality factor. Simultaneously with this energy transfer, wave momentum will also be transferred to the mean flow (Longuet-Higgins, 1953; Jenkins, 1987, 1989). The effect of waves on the momentum flux through the air–sea interface is discussed by Janssen (1989), Jenkins (1992) and Jenkins (1993). This momentum flux will not be directly assessed with the present simulation. Depending on the observational technique for near-surface turbulence, various parameterisations have been suggested for z_0. Based on observations from fixed towers, where the surface reference is the mean surface elevation, Terray et al. (1999) suggest $z_0 = H_s$ with the significant wave height H_s. In contrast to that, Gemmrich and Farmer (1999) find much smaller values for z_0 with an instrument floating with the waves and thus having the momentary sea surface as the reference. For significant wave heights of about 5 m, they found $z_0 \approx 0.2$ m. Gemmrich and Farmer (2004) confirmed that result. As we use a freely rising profiler equipped with a pressure sensor, referencing to the momentary surface elevation, we expect z_0 to H_s ratios similar to Gemmrich and Farmer (1999).

In this paper we address two main aspects of this continuing debate: Firstly we present microstructure data of the SBL from a fetch-limited wind-exposed lake, where significant turbulence has been observed (Simon, 1997; Sander et al., 2000; Lorke and Wüest, 2002). It will be shown that also for this special situation of short and young breaking waves there exists a well-defined WASL with enhanced dissipation. In addition, we thereby demonstrate that the often criticised profiling method (Gibson, 1982) captures the WASL despite the large intermittency. Until now, practically only Soloviev et al. (1988) and Anis and Moum (1995) used the vertical profiling technique for this purpose. Secondly, we want to test whether the improved model by Burchard (2001a) is able at reproducing the turbulence measurements taken under those specific conditions of short and young waves. As an additional test, we investigate specifically the lower range of wind speeds and examine the vertical slope of turbulent dissipation rate in the WASL. As the unmodified k–ε model has been many times tested rigorously against different sets of measurements (Burchard and Bolding, 2002; Stips et al., 2002; Simpson et al., 2002), we refrain from any tuning of parameters of the model.

The improved two-equation k–ε turbulence model by Burchard (2001a) is explained in Section 2, the measurement setup is described in Section 3, whereas the data from the measurements and from the simulations are presented in Section 4, before they are finally discussed in Section 5.

2. Model description

The mathematical model on which the numerical simulations are based, consists of six dynamical equations for the two Reynolds averaged velocity components u (eastward) and v (northward), the averaged potential temperature T, the averaged salinity S, the turbulent kinetic energy k and the turbulent dissipation rate ε:

$$
\begin{aligned}
&\partial_t u - \partial_z((\nu_t + \nu)\partial_z u) = fv,\\
&\partial_t v - \partial_z((\nu_t + \nu)\partial_z v) = -fu,\\
&\partial_t T - \partial_z((\nu_t' + \nu')\partial_z T) = \frac{1}{C_p \rho_0}\partial_z I,\\
&\partial_t S - \partial_z((\nu_t' + \nu'')\partial_z S) = 0,\\
&\partial_t k - \partial_z\left(\frac{\nu_t}{\sigma_k}\partial_z k\right) = P_S + P_B - \varepsilon,\\
&\partial_t \varepsilon - \partial_z\left(\frac{\nu_t}{\sigma_\varepsilon}\partial_z \varepsilon\right) = \frac{\varepsilon}{k}(c_1 P_S + c_3 P_B - c_2 \varepsilon),
\end{aligned}
\tag{1}
$$

with gravitational acceleration g, averaged density ρ and the Coriolis frequency $f = 2\omega\sin(\phi)$ with the earth's angular velocity ω and latitude ϕ. In the potential temperature equation, further terms are solar radiation I in the water column

(generally calculated from the given surface radiation as an exponentially decreasing function with depth), the specific heat capacity of water C_p, and a reference density ρ_0. The molecular diffusivities for momentum, temperature and salinity are given by ν, ν' and ν'', respectively. The coordinates are x (eastward), y (northward), z (upward) and t (time). In addition to the system of Eqs. (1), the UNESCO equation of state for calculating the potential density as functions of T, S and hydrostatic pressure is applied. Shear production of turbulence is denoted as $P_S = \nu_t((\partial_z u)^2 + (\partial_z v)^2)$ and buoyancy production as $P_B = \nu'_t(g\rho_0)\partial_z\rho$. Eddy viscosity and eddy diffusivity are denoted by ν_t and ν'_t, respectively.

The first four equations of (1) for velocity components and active tracers are the so-called hydrostatic primitive equations with some further simplifications. Horizontal homogeneity is assumed with the consequence that all horizontal gradients such as pressure gradients and advective terms vanish. It will be discussed later that this assumption is crude near the shore, but however necessary due to lacking information on such gradients.

The turbulence closure needed to calculate ν_t and ν'_t is obtained from applying a Reynolds decomposition into a mean and a fluctuating part of the flow and tracer fields and to construct transport equations for the second-order correlators of fluctuations. After assuming local equilibrium for these correlators and closing the remaining unknowns by empirical assumptions, eddy viscosity and diffusivity result as (Burchard, 2002)

$$\nu_t = c_\mu \frac{k^2}{\varepsilon}, \quad \nu'_t = c'_\mu \frac{k^2}{\varepsilon}. \tag{2}$$

Here, c_μ and c'_μ are non-dimensional stability functions, depending on shear frequency, Brunt–Väisälä frequency and the turbulent time scale, k/ε. We use here the set of stability functions which has recently been suggested by Canuto et al. (2001) and validated against mixed layer observations by Burchard et al. (2000).

The equations for turbulent kinetic energy k and its dissipation rate ε are needed for two reasons: (i) calculating the vertical eddy viscosity and diffusivity ν_t and ν'_t by means of (2) and (ii) reproducing the observed dissipation rate ε. These equations for k and ε result from the Reynolds decomposition discussed above.

Starting from the standard prognostic equation for turbulent kinetic energy (fifth equation of (1)), Craig and Banner (1994) suggested an analytical solution for the wave enhanced layer by assuming a positive surface flux of TKE due to energy injection by breaking surface waves and a balance of viscous dissipation with vertical TKE transport (thus neglecting shear production of TKE). Since this is realistic only very close to the surface, Craig (1996) extended this study by including shear production for which he found an approximate analytical solution. When prescribing the macro length scale as $L = \kappa d$ with the non-dimensional distance $d = (z_0 - z)/z_0$ from below an unresolved surface layer of thickness z_0 (with the vertical coordinate z pointing upwards) and prescribing the surface TKE flux as $F_s(k) = c_w|u_*|^3$ (with the empirical non-dimensional parameter c_w, which theoretically depends on wave age and the surface friction velocity u_*) the analytical solution including the WASL reads as

$$\begin{aligned} k_{\mathrm{WASL}} &= k_{\mathrm{LOW}}(1 + c \cdot d^{-m})^{2/3} \\ \varepsilon_{\mathrm{WASL}} &= \varepsilon_{\mathrm{LOW}}(1 + c \cdot d^{-m}) \end{aligned} \tag{3}$$

with the empirical non-dimensional parameters m and $c \propto c_w$. Here, $k_{\mathrm{LOW}} \propto u_*^2$ and $\varepsilon_{\mathrm{LOW}} \propto |u_*|^3 d^{-1}$ denote the LOW solutions. Since the vertical decay of $\varepsilon_{\mathrm{LOW}}$ is $\propto d^{-1}$, the decay of $\varepsilon_{\mathrm{WASL}}$ near the surface is given as $\propto d^{-(m+1)}$. The parameter m depends on the Schmidt number for TKE, σ_k, the von Kàrmàn parameter κ and the ratio of surface friction velocity squared to TKE, c_μ. Using standard parameters for the TKE equation from various sources (e.g. Mellor and Yamada, 1974; Rodi, 1980), the vertical decay rate $-(m+1)$ falls into the empirical range of -2.3 ± 0.4. For the Canuto et al. (2001) stability functions however, $-(m=1) = -3.2$ (see Appendix A) which is outside the empirical range.

The flux of momentum from the atmosphere into the sea is calculated by means of bulk

formulae developed by Smith (1988):

$$(\nu_t \partial_z u)_s = c_d \frac{\rho_a}{\rho_0} U_{10}(U_{10}^2 + V_{10}^2)^{1/2};$$
$$(\nu_t \partial_z v)_s = c_d \frac{\rho_a}{\rho_0} V_{10}(U_{10}^2 + V_{10}^2)^{1/2}, \quad (4)$$

with the wind velocity vector at 10 m height, (U_{10}, V_{10}), the air density, ρ_a, the water density, ρ_0 and the dimensionless drag coefficient c_d, calculated by the bulk formula. It should be noted that the direct flux of momentum (and consequently mean kinetic energy) and TKE from the atmosphere to the sea is a highly idealised view. In reality, first energy is transferred to the surface wave field which is then transferring simultaneously mean and turbulent kinetic energy into the sea (Longuet-Higgins, 1953; Jenkins, 1987). Thus, the drag coefficient c_d and the parameter c_w are strongly correlated and should consequently be based on the same theoretical assumptions. However, such a unifying theory has not yet been developed. Another simplification implicitely included in the bulk formula approach is that momentum is only transferred at the sea surface, although momentum transfer from waves to the mean flow occurs as a body force in the upper few metres (scaled by the wave length). This is partially parameterised in the present approach by calculating the near-surface eddy viscosity as function of the injected TKE, such that momentum transfer due to turbulent mixing is increased.

The parameters contained in the ε equation are fitted to various empirical laws, see Umlauf and Burchard (2003) for a review. One of them, the Schmidt number σ_ε is fitted such that the LOW is a solution for steady-state constant stress conditions. It could however also be fitted to pure WASL conditions (no shear production), but then the LOW conditions would be excluded. Since the parameters c_1–c_3 are already used for reproducing other flow properties, no degree of freedom is left for including the WASL and LOW conditions in one model. Since pure WASL conditions are characterised by $P_S/\varepsilon \to 0$ and pure LOW conditions by $P_S/\varepsilon = 1$, Burchard (2001a) suggested to calculate the Schmidt number for ε as

$$\sigma_\varepsilon = \max\left\{0, 1 - \frac{P_S}{\varepsilon}\right\}\sigma_{\varepsilon,\mathrm{WASL}} + \min\left\{1, \frac{P_S}{\varepsilon}\right\}\sigma_{\varepsilon,\mathrm{LOW}} \quad (5)$$

and could show that the resulting numerical solution approximated the Craig (1996) analytical solution very well.

The present turbulence model uses the empirical parameters given in Table 1. The turbulent Schmidt number for the turbulent kinetic energy, $\sigma_k = 1$ is a rough estimate (e.g. Rodi, 1980), the turbulent Schmidt numbers for the dissipation rate, $\sigma_{\varepsilon,\mathrm{WASL}}$ and $\sigma_{\varepsilon,\mathrm{LOW}}$ depend on various other parameters (Section 7), c_1 and c_2 result from laboratory experiments with homogeneous shear flow and grid turbulence, respectively. For stable stratification, c_3 results from fitting the steady-state Richardson number to idealised experiments (Burchard and Baumert, 1995; Burchard et al., 2000), for instable stratification, c_3 needs to be positive in order to retain a source of dissipation rate also for free convection (Rodi, 1980). In order to obtain positive definite solutions for the stability functions c_μ and c'_μ, certain realisability constraints have to be considered, see Burchard and Deleersnijder (2001).

The numerical discretisation of the model is described in detail by Burchard et al. (1999) and Umlauf et al. (2005). In order to obtain numerically stable results for this mainly wind driven scenario, a time step of $\Delta t = 10$ s has been used. The vertical resolution was not equidistant, as we used slight zooming to the surface. The mean vertical step size was about $\Delta z = 0.15$ m. The model was initialised on March 9 1996 at 00:00 h with the first observed profiles of temperature and

Table 1
Empirical constants for the extended k–ε model by Burchard (2001a) with the Canuto et al. (2001) second-moment closure

σ_k	$\sigma_{\varepsilon,\mathrm{LOW}}$	$\sigma_{\varepsilon,\mathrm{WASL}}$	c_1	c_2	c_3 $(N^2>0)$	c_3 $(N^2<0)$	κ	c_w
1.0	1.2	2.01	1.44	1.92	−0.629	1.0	0.4	100

salinity (Section 3), zero velocities and k and ε set to minimum values. The model simulation terminates on March 20 at 13:00 h when the last vertical profile was observed.

The height of the unresolved wave-turbulent sublayer z_0 (also called surface roughness length) has to be prescribed as additional external model parameter. Burchard (2001a) has shown that an adaptation of the Charnok (1955) formula

$$z_0 = \alpha u_*^2/g \tag{6}$$

with the dimensionless parameter $\alpha = 1400$, Craig and Banner (1994), resulted in a satisfactory simulation of available observations. Therefore we used Eq. (6) as a starting point for the simulations and investigated further the sensitivity of the model to the roughness length z_0, by using different values for the parameter α (e.g. 5600, 14,000, 56,000).

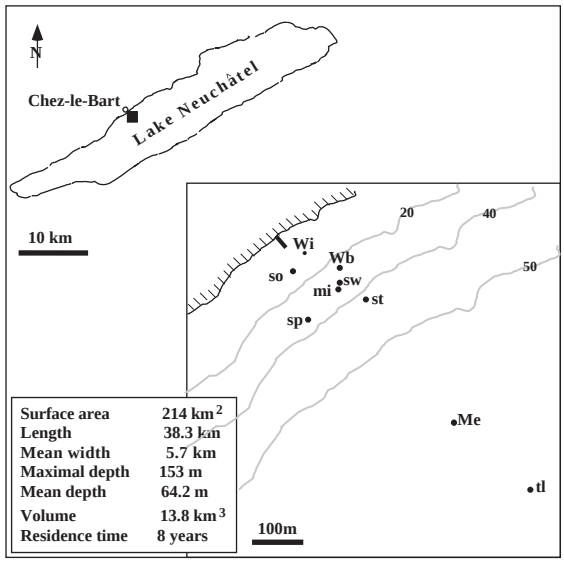

Fig. 1. Lake Neuchâtel, Switzerland. The measurement location was at the shore of Chez le Bart. The meaning of the abbreviations for the different used instruments is given in Table 2.

3. Observations

3.1. Study site and experimental setup

The measurements were carried out in Lake Neuchâtel, located in the western part of the Swiss Plateau. The lake is approximately rectangular, with its longest axis directed SW–NE. It has a volume of 13.8 km^3, a surface of 214 km^2 and a maximum depth of 153 m. The experiment took place during 12 days from March 9–20, 1996. We have chosen a measurement place located at the shore of Chez le Bart (46°53,883′N, 6°47,383′E, Fig. 1). The particular location for the experiment was selected for its wind exposure, the absence of major river inlets and a steep shore line to allow the safe mooring of the instrumentation (Simon, 1997).

In order to measure the atmospheric forcing, wave heights and turbulence, we operated a meteorological station on a buoy ≈ 2 km off-shore and a moored pressure gauge and two microstructure profilers ≈ 300 m off-shore, see Fig. 1. Meteorological data (wind speed, wind direction, buoy orientation, air temperature, relative humidity, solar radiation and global radiation) were measured by an autonomous meteorological station AMS 2700 (Aanderaa Instruments, Bergen, Norway) at 2.8 m height above lake surface every 2 min. Near to the location of the microstructure probes an additional anemometer was placed at 0.95 m above lake surface (Fig. 1). For general background information thermistor strings and current meters were moored.

Microstructure profiles were collected by using two completely different probes, sensing small-scale temperature and current shear (see below). This allowed to estimate and compare dissipation of TKE from two independent systems (Kocsis et al., 1999). These probes were connected via special winches to data acquisition and control computers at the shore base. The locations of the respective instruments, as well as their abbreviations used in Fig. 1 is detailed in Table 2.

3.2. Microstructure measurement technique

Two profilers were operated in quasi freely-rising mode, to infer TKE dissipation rates: The MST profiler of the Joint Research Centre (Ispra, Italy) (predecessor of the MSS profiler as produced by Sea & Sun Technology and ISW

Table 2
Location and respective abbreviation of the moorings in Fig. 1 during the Lake Neuchâtel field experiment 1996

Sensor	Longitude	Latitude	Abbreviation
Currentmeter 5 m	6° 47′26.7	46°53′51.6″	st
Currentmeter profiling	6° 47′19.0″	46°53′48.5″	sp
Currentmeter surface	6° 47′17.0″	46°53′55.9″	so
Microstructure temperature	6° 47′23.2″	46°53′54.2″	sw
Microstructure shear	6° 47′23.0″	46°53′53.1″	mi
Wave gauge	6° 47′23.2″	46°53′56.4″	Wb
Wind buoy	6° 47′19.0″	46°53′58.6″	Wi
Meteo buoy	6° 47′38.4″	46°53′32.6″	Me
Thermistors string	6° 47′48.5″	46°53′22.2″	tl

Wassermesstechnik, Germany) and a temperature microstructure profiler based on SeaBird (Bellevue, USA) sensors and electronic boards, owned by EAWAG.

The MST profiler was equipped with microstructure temperature and current shear sensors, as well as conventional CTD-sensors. The microstructure temperature sensor is based on a microthermistor FP07 (Thermometrics, USA) with a nominal response time of about 7 ms. For the microstructure shear measurements, the profiler was equipped with a PNS shear sensor (Prandke and Stips, 1998). The standard temperature sensor is of the Pt100 type and has an accuracy of $\pm 0.01\,^{\circ}C$. For the electrical conductivity measurements a 7-pole cell with an accuracy of $\pm 0.01\,mS\,cm^{-1}$ is used. The piezo-resistive pressure sensor has an accuracy of ± 10 cm. The resolution for all sensors is determined by the used 16 bit analog digital converter. The sampling rate for all sensors was 1024 Hz. The system enables the measurement of small-scale current shear with a vertical resolution down to about 5 mm. The mechanical construction, the electronics and the basic signal processing are described in detail by Prandke and Stips (1998) and in the references cited therein.

The temperature microstructure profiler is an adapted SeaBird SBE-9 CTD profiler. It was equipped with a pair of such FP07 thermistors. The sampling frequency was 96 Hz. Details of the profiler construction as well as the processing and analysis of the temperature microstructure data are described in Simon (1997), Kocsis et al. (1999) and Lorke and Wüest (2002).

For the rising measurements the winch was placed at the shore and a guide pulley was used about 300 m away from the shore at a water depth of 38 m. To reduce the influence of cable vibrations on the profiler, the cable of the MST profiler was pulled by an additional buoyancy ball equipped with a pressure sensor, at about 6 m below the profiler. Data were recorded between 30 and 0 m depth. One single cast was done every 15 min, resulting in a total of more than 1100 casts.

Dissipation rates from both profilers were found to agree satisfactorily (Kocsis et al., 1999). There from it can be concluded that the temperature microstructure method using standard thermistors, is suitable for resolving low dissipation rates (smaller $10^{-10}\,m^2\,s^3$), but seems to underestimate dissipation rates above $10^{-7}\,m^2\,s^3$. As the focus of this work is the very near surface region having higher dissipation rates, we decided to use here the dissipation rate data from the MST profiler alone.

3.3. MST data processing and reduction

The shear data processing followed the commonly used procedure for shear calculation as described by Stips and Prandke (2000). Spiky data were detected and removed by a filter which determines the local variance of the signal. Low frequency disturbances as well as high frequency noise was removed by a bandpass filter. Overlapping depth segments of 0.3 m length were used to calculate the shear variance and to estimate the dissipation rate ε. The length of the uppermost bin is reduced to 15 cm, which will provide a dissipation rate estimate at 0.075 m depth. The second bin is located at 0.15 m. For the spectrum integration the lower wavenumber bound k_L is 2 cpm, which is set by the 1 m length of the profiler. The upper wave number bound k_U is determined by an iterative procedure (Prandke and Stips, 1998). Assuming isotropy of the small-scale turbulence the dissipation rate ε [$m^2 s^{-3}$] was then estimated

through

$$\varepsilon = 7.5\nu\overline{(\partial_z u')^2}. \quad (7)$$

Here, $\partial_z u'$ is the vertical profile of the current shear fluctuations. Finally, the dissipation rate is corrected for the lost variance below and above the used integration interval and for the limited spatial response of the sensor. The overbar denotes ensemble averaging, which is here replaced by spatial/temporal averaging. A detailed discussion of the errors involved in the estimation of ε is found in Moum and Lueck (1985). The error estimate for the present application is, that ε was determined within a factor of 2, when above

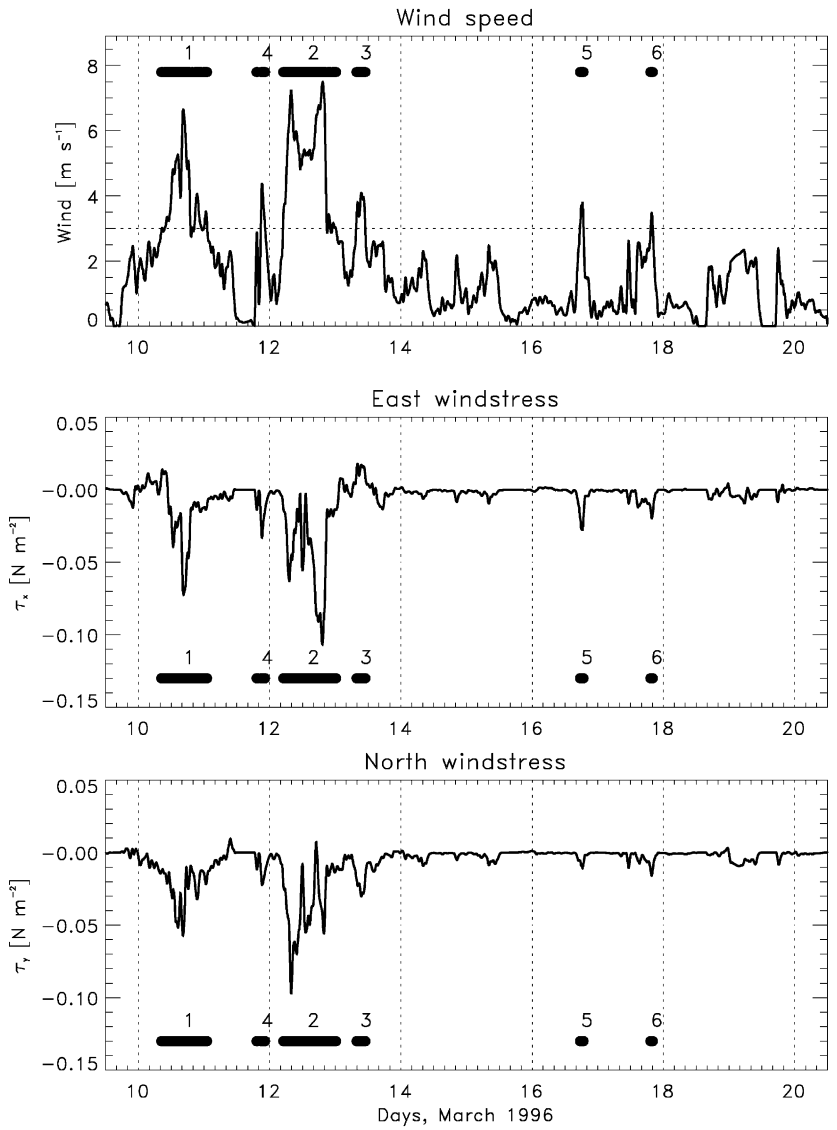

Fig. 2. Wind speed at the small buoy (upper panel), East wind stress (middle panel) and North wind stress (lower panel) as measured at Lake Neuchâtel. The six classified wind events with wind speeds exceeding $3\,\mathrm{m\,s^{-1}}$ are marked by bold lines and the corresponding event number. The two major events (1,2) at 10 and 12 of March can be clearly identified. The long tick marks correspond to the beginning (midnight) of the indicated day.

$10^{-9}\,m^2\,s^{-3}$. The short cable between profiler and buoyancy body, hanging below the profiler generated vibrations. Because these vibrations contaminated the spectra, the noise threshold was $3\times10^{-10}\,m^2\,s^{-3}$.

To avoid calculating unrealistic dissipation rates when the shear sensor is already in air, the determination of the exact surface point is important. This transition point was automatically determined from the signal of a fast conductivity sensor, the fast thermistor and the abrupt change within the shear signal. After manual inspection of the respective sensor signals, each profile was cut at that point. The uncertainty of the surface point, is better than ±1 cm. The pressure signal was used to calculate the profiler velocity. As this signal is influenced by waves near the surface, a linear least square fit of the pressure data was done. By allowing only linear changes of the pressure in the uppermost 5 m, the wave signal was effectively removed.

3.4. Wind forcing

In order to get meteorological data which reflect the atmospheric conditions of the open water, the meteorological station was moored ≈2 km from the shore (Fig. 1). Wind velocities measured at 2.8 m above the water surface, were rescaled to the standard height of 10 m. During the microstructure data collection, the mean wind speed was $3.2\,m\,s^{-1}$ at the meteorological buoy. This constant low velocity was interrupted on two occasions, lasting for approximately one day, when the wind speed exceeded $6\,m\,s^{-1}$ (Fig. 2). The first occasion was on March 10/11 and the second occasion on March 12/13, when the maximum wind gusts, recorded reached $14.6\,m\,s^{-1}$ around midnight.

Until March 14, NNE-winds prevailed (~73% of all wind direction measurements) indicating that the wind was parallel to the lake. Especially during the two main events, wind blew almost parallel to the main axis of the lake and had subsequently a long fetch. After March 14, winds exceeding $4\,m\,s^{-1}$ occurred as short gusts of less than one hour duration. Their directions were mainly from NNW and subsequently had short fetches. Therefore the most interesting period will be the four days episode of March 10–13, when wind was high as well as variable and the fetch was long.

Wind speed was additionally measured by a small buoy about 90 m away from the microstructure probe locations with an anemometer at a height of 95 cm above the water surface. The accuracy of this anemometer is $\pm0.1\,m\,s^{-1}$. This additional measurement allowed us to access the wind speed directly at the place of the dissipation rate sampling. By comparing near shore and off shore wind velocities we got evidence for the importance of frictional effects at the topography, which led to a reduction of wind speed by 40% near the shore compared to the open lake values. Therefore we used this near-shore wind speed for simulating the dissipation rate. Wind stress was calculated from wind speed measured at the small buoy using the Smith (1988) bulk formula (Fig. 2). In this iterative procedure the scaling to 10 m reference height and the calculation of the drag coefficient are included.

Further, individual wind events, with wind speed exceeding $3\,m\,s^{-1}$ have been identified in Fig. 2 and Table 3. The critical wind speed of $3\,m\,s^{-1}$ was used, as above this wind speed first whitecaps have been observed. For later reference each of these events is given a number which is listed together with duration, mean wind stress and mean wind speed in Table 3. The duration of the identified event 6 was rather short (<60 min), but wind speeds between 2 and $3\,m\,s^{-1}$ prevailed for several hours prior to reaching the threshold of $3\,m\,s^{-1}$.

Table 3
Table of identified events, having wind speeds above $3.0\,m\,s^{-1}$ at the small meteorological buoy

Event	Start	End	Duration	Stress	Speed
—	UTC	UTC	h	$N\,m^{-2}$	$m\,s^{-1}$
1	10.347	11.047	16.80	0.039	3.81
2	12.207	13.013	19.33	0.065	4.97
3	13.324	13.460	3.27	0.029	3.41
4	11.800	11.932	3.17	0.031	3.47
5	16.729	16.785	1.33	0.027	3.29
6	17.801	17.839	0.90	0.024	3.11

Start time and end time are days of March 1996. Events 1 and 2 are classified as major wind events, the others (3–6) are minor wind events.

3.5. Surface waves

Surface waves were measured with a pressure transducer located 1.0 m below the surface and anchored at 40 m depth. Pressure was recorded at 4 Hz and with 1.5 cm resolution within a distance of about 100 m from the two microstructure profilers, see Fig. 1. From the time series of pressure, wave height spectra were calculated for ~8 min long records and, after correcting for the installation depth of the sensor (Bishop and Donelan, 1987), the significant wave height H_S [m] and the peak frequency f_p [s^{-1}] was calculated (Simon, 1997).

According to the wind direction, the maximum fetch was nearly half of the lake length and was therefore long enough to induce considerable wave height, see Fig. 3. Recorded wave heights reached a maximum of 66 cm on March 10, shortly after wind speed had its maximum. Two major wave events during March 10 and March 12 with $H_S > 20$ cm can be identified from the wave measurements, see lower bold lines in Fig. 3.

During the second half of the experiment, the fetch and the duration were too short to build up waves with a significant wave height of more than 0.08 m (Fig. 3). The peak frequency f_p varied between about 0.55 Hz for weak wind and 0.2 Hz for strong wind. These frequencies correspond to wave phase velocities between $c_p = g/(2\pi f_p) \approx 3$ and 8 m s^{-1}. The corresponding wave numbers $k_p = (2\pi f_p)^2/g$ and wavelength $\lambda_p = 2\pi/k_p$ were between 1 m^{-1} and 0.14 m^{-1} and between 5 and 40 m, respectively.

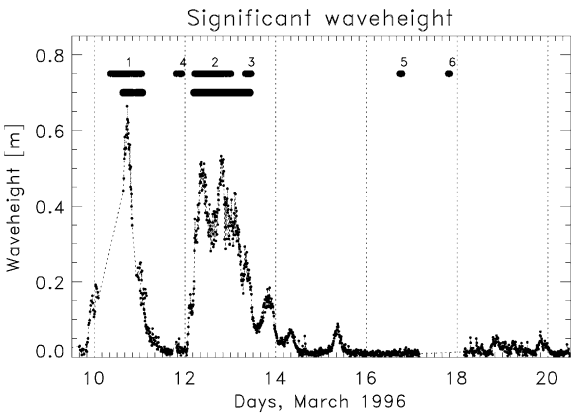

Fig. 3. Significant waveheight H_S measured at about 50 m distance from the turbulence profiling equipment during the Lake Neuchâtel experiment. The six classified wind events are marked by the upper bold lines. Two time periods having a significant waveheight H_S of greater than 20 cm are marked by the lower bold lines.

The depth dependence of the wave orbital motion leads to a Lagrangian velocity, which is named after its first investigator Stokes drift u_s (see Stokes, 1847). For monochromatic waves the Stokes drift decreases with depth as given by Skyllingstad and Denbo (1995):

$$u_s = (kH_S/2)^2 \sqrt{g/k} e^{-2kz}. \quad (8)$$

Typical values for the stokes drift during the wind events at about 7.5 cm depth (which is the mean depth of the uppermost bin for which a dissipation rate value is calculated) are between 2 and 7 cm s^{-1}, see Table 4.

3.6. Heat flux and temperature structure

Heat flux H_{net} was calculated from standard bulk formula (Henderson-Sellers, 1986) and using the available shortwave measurements. H_{net} varied during the experiment between −340 and 600 W m^{-2} with a mean heat input of ~48 W m^{-2}, see Fig. 4. Surface heat flux in Fig. 4 is the sum of sensible, latent and net longwave radiative heat flux.

Until March 14, the mean temperature of the lake decreased during the nights with negative heat fluxes between −340 and −30 W m^{-2}. Afterwards, with one exception at March 16 the net heat flux remained positive. Initially the experimental site was thermally stratified, but after the second wind event March 14 the water column was practically homogeneous. Thermal stratification reestablished after March 15, see Fig. 5. The stability of the water column expressed as buoyancy frequency squared $N^2 = -(g/\rho)\partial\rho/\partial z \approx 10^{-5}\ s^{-2}$ was generally low as both the temperature gradients and thermal expansivity α were small. Only in the top 3 m, N^2 exceeded $10^{-4}\ s^{-2}$. Below, the stability was less than $2 \times 10^{-5}\ s^{-2}$ until March 14. Afterwards, when wind generally ceased and the heat flux

Table 4
Table of wave parameters for the previously identified wind events, having wind speeds above 3.0 m s^{-1}

Event	Height	Peak frequency	Wavenumber	Stokes drift	Energy
—	H_S [m]	f_P [Hz]	k [m^{-1}]	u_S [m s^{-1}]	E_W [J m^{-2}]
1	0.43	0.42	0.72	0.070	111.7
2	0.40	0.35	0.50	0.039	95.7
3	0.22	0.45	0.80	0.024	30.2
4	0.022	0.44	0.79	0.000	0.3
5	0.01	0.45	0.83	0.000	0.1

Height H_S is used for significant wave height. Stokes drift is estimated at a depth of 7.5 cm. There are no wave measurements for wind event 6 available. Only the first 3 wind events have significant waveheights above 20 cm.

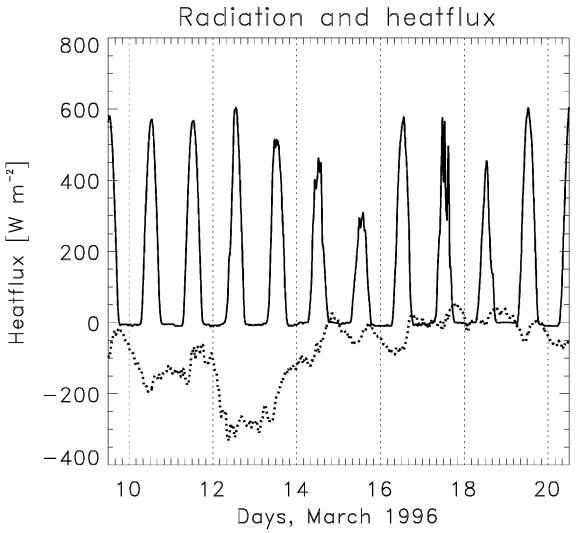

Fig. 4. Short wave radiation (upper solid curve) and surface heat flux (lower dotted curve) as respectively measured and calculated during the Lake Neuchâtel field experiment. The surface heat flux is the sum of sensible, latent and net longwave radiative flux.

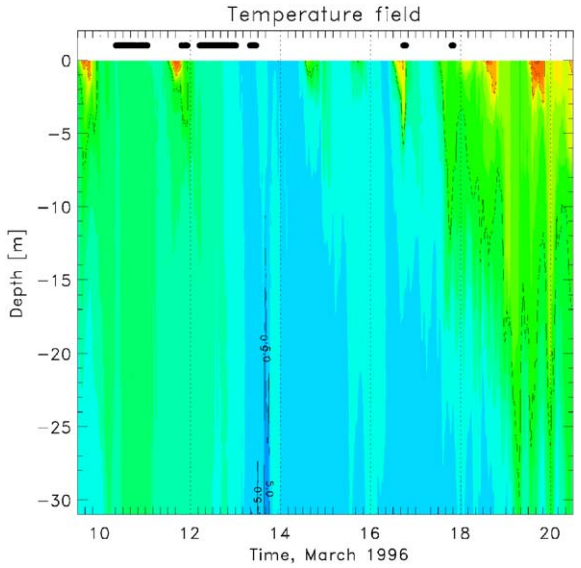

Fig. 5. Contour plot of measured temperature field during the Lake Neuchâtel field experiment. Contours span the range from 5.0 °C (blue) to 6.2 °C (red).

became positive (into the lake), stability increased throughout the SBL and N^2 reached $\sim 3 \times 10^{-5}$ s^{-2} for the bulk of the SBL.

In the bulk of the water column the temperature was all the time between 5 and 6 °C (Fig. 5). Only during short periods of sun shine the near surface layer reached temperatures above 6 °C, see the red spots in Fig. 5. Initial temperature stratification was destroyed after wind event 1 on March 10, reestablished March 11, but was destroyed during wind event 2, March 12. Even the contribution to mixing of the minor wind events 5 and 6 can be seen in Fig. 5. After March 15 the temperature stratification increased gradually until the end of the experiment. Following the storm during March 12/13 colder water of about 5.2 °C entered the measuring site. As this colder water was not produced by the local heat loss, it must have been advected to the measurement place.

3.7. Dissipation of turbulent kinetic energy

During the course of the experiment, turbulence was dominated by wind, as the surface buoyancy flux was small. During the two periods of strong cooling March 10 and 12, wind was especially heavy and therefore wind generated turbulence exceeded the surface buoyancy flux which averaged at $\sim 1 \times 10^{-8}\,m^2\,s^{-3}$ that night. In Section 5 it is shown that production of TKE due to wind/wave forcing during the strong wind events was up to about 3 orders of magnitude larger than TKE production due to the surface buoyancy flux. The measured dissipation values varied over 5 orders of magnitudes from $\varepsilon \sim 10^{-10}$ to $\varepsilon \sim 10^{-5}\,m^2\,s^{-3}$ and averaged at $2 \times 10^{8}\,m^2\,s^{-3}$ over the top 30 m. Within the usual scatter due to intermittency, dissipation followed the wind forcing, see Section 4. Further, as a function of depth, dissipation resembled LOW scaling, which implies $\varepsilon \sim z^{-1}$. This will be discussed in more detail below.

4. Comparison of measured and simulated data

In this section we will compare the results from the observations with the performed simulations.

In order to assess the importance of advection and wave breaking for the experiment, different runs were performed. Run r1 applied the unmodified k–ε model forced by surface heatflux and wind stress, without wave breaking parameterisation and without relaxation of temperature. As advection was important during the experiment, the run rl did not provide a realistic simulation, and results from this run will not be considered further. As our aim is not to reproduce the dynamics of the temperature field, but to focus on the near surface turbulence, we decided to relax the simulated temperature field to the measured temperature profiles. Therefore we used for run r2 again the unmodified k–ε model, but in this case with relaxation. In run r3 the Craig and Banner (1994) wave parameterisation was activated. Additionally for run r4 the surface roughness length z_0 was increased by a factor of 10. Different sensitivity tests were done, which will be only briefly mentioned, when necessary.

4.1. Dissipation rate field

Observed and simulated dissipation rates (run r2) in the depth interval 30 to 0 m are shown in Fig. 6. We find that all the major and minor wind events during the experiment lead to enhanced near surface dissipation rates in the measurements, as well as in the simulated ε. During the major wind events increased dissipation rates can be found down to the maximal depth at which measurements were made (30 m), but even the minor wind events show higher dissipation rates down to about 20 m. Run r2 shows an acceptable simulation, as the higher dissipation rates produced during the major wind events are extending down to 30 m in accordance with the measurements. More over, especially during the minor wind

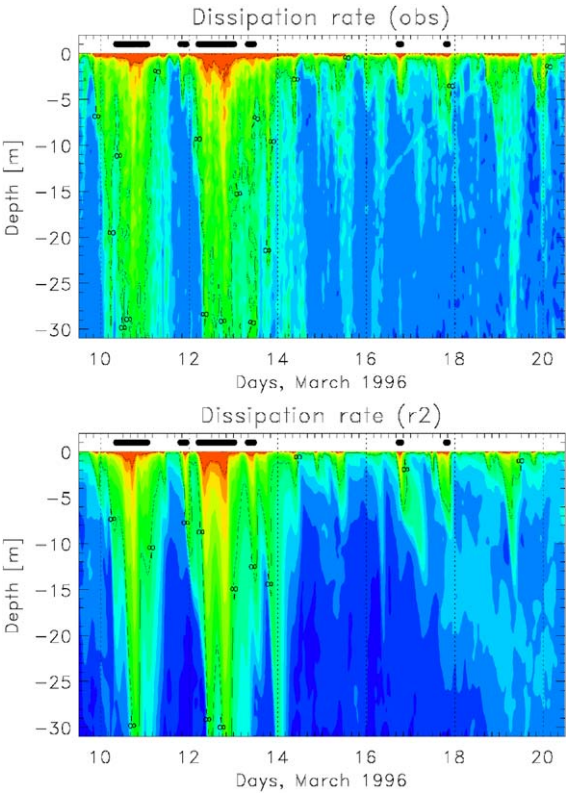

Fig. 6. Contour plots of decadal logarithm of dissipation rate fields, measured (upper panel) and simulated with relaxation run r2 (lower panel). The range is from $\log(\varepsilon) = -6$ (red) to $\log(\varepsilon) = -10.6$ (dark blue) and the wind events are indicated by the bold lines.

events the increased levels of observed dissipation rates reach deeper than in the simulations. Further, the model needs much more time to increase dissipation at about 30 m. This is likely due to the additional effect of vertical convection during the nocturnal cooling, which results in a downgradient flux of TKE. This convective flux is only to first order parameterised within GOTM (Stips et al., 2002) and is not well reproduced. Also the small-scale variability in the measurements is higher than in the simulation. This is caused by the intermittency in the measurements, which is excluded in the used type of turbulence model. Run r3 and run r4 would not show evident differences to run r2 in this overview plot and are not shown. Therefore we are forced to look into the details at the near surface to see possible effects of wave breaking.

4.2. Time series of dissipation rate

The time series of the averaged near surface dissipation in the uppermost meter is shown in Fig. 7. The simulated near surface dissipation rates, without consideration of wave breaking (run r2), underestimates the measured ones during most of time quite considerable. Applying the wave breaking parameterisation (run r3), most of the wind events are adequately reproduced.

Rather well reproduced are the major wind event 2 and the minor wind events 3, 5 and 6. The performed simulation of the wind events 1 and 4 match less well with the data. Wind event 1 has rather specific characteristics as the wind is increasing and changing direction from NW to NE. Wind event 4 is a gust, which did not lead to any significant wave development (3). This is the only case, were simulated dissipation rates exceed the observed ones. A interesting case occurred at March 15, when wind was only $\approx 2\,\mathrm{m\,s^{-1}}$, but wave heights reached nearly 10 cm. In this case observed dissipation rates were similar to event 5 and 6. This opposite behaviour cannot be explained from the available data. During March 13, when the wind was decaying, observed dissipation rate exceeds all simulations nearly at all times. On most other occasions observed ε responded with a quick decrease to decaying wind, as e.g. on March

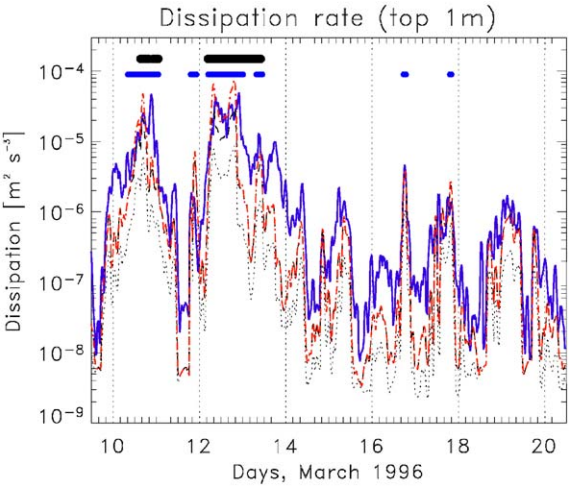

Fig. 7. Mean dissipation rate in the uppermost 1 m, measured (blue solid line), run r2 (dotted line), run r3 (dashed line) and run r4 (red dash–dot line). Except during the strongest winds of event 1 and 2, the results from run r3 and r4 cannot be distinguished. The two major wave events with wave height greater than 20 cm are marked bold black. The respective wind events are marked by the smaller bold blue lines.

11, 14, 15, 17 and 19. The major difference between these events is, that waves were existing during March 13, but not on the other occasions. Therefore it looks like an existing wave field would maintain larger dissipation rates.

Considering only the selected wind events, we can suspect, that the well simulated wind events are characterised by wind having rather constant magnitude and direction. The improvement due to an increased surface roughness length (run r4), can be hardly seen on the scale of this plot. Only during very limited time periods, the black line from run r3 can be identified at lower levels compared to run r4 (red line). The influence of the duration of the wind seems not so clear, as e.g. wind events 4 and 5 have similar duration, the wind is coming from the same direction, both show no significant wave development, but only event 5 is well reproduced.

Analysing the correlation between the logarithm of the measured and simulated surface dissipation rates (Table 5), we find a slightly better correlation for runs r4 and r3 compared to run r2. Further the

linear regression curve approaches more closely the ideal slope of 1.

Table 5
Results of the linear regression analysis between logarithm of measured and simulated dissipation rates of the uppermost meter (runs r2, r3 and r4)

Run	a_0	a_1	r	σ	χ^2
r2	−2.02	0.84	0.85	0.016	277.8
r3	−0.97	0.94	0.87	0.016	297.8
r4	−0.65	0.98	0.87	0.017	336.3

Here a_0 denotes the constant, a_1 the slope, r the correlation coefficient, σ the standard error of the fit and χ^2 is the value for χ-square-goodness-of-fit test.

4.3. Near surface slope of dissipation rate

The near surface slope of the dissipation rate, averaged over the duration of the different identified wind events, is shown in Fig. 8. The black circles are the results from the simulation without (r2), black dots are with wave breaking (r3) and the red dots are from run r4 with increased surface roughness length. The blue dots are mean values calculated from the measured data. In all 6 cases there is a clear improvement of the simulated dissipation rate using the wave breaking parameterisation (r3) compared to the unmodified k–ε model (r2). The major wind events 1 and 2 are even better reproduced, when using an increased surface roughness length, as done for

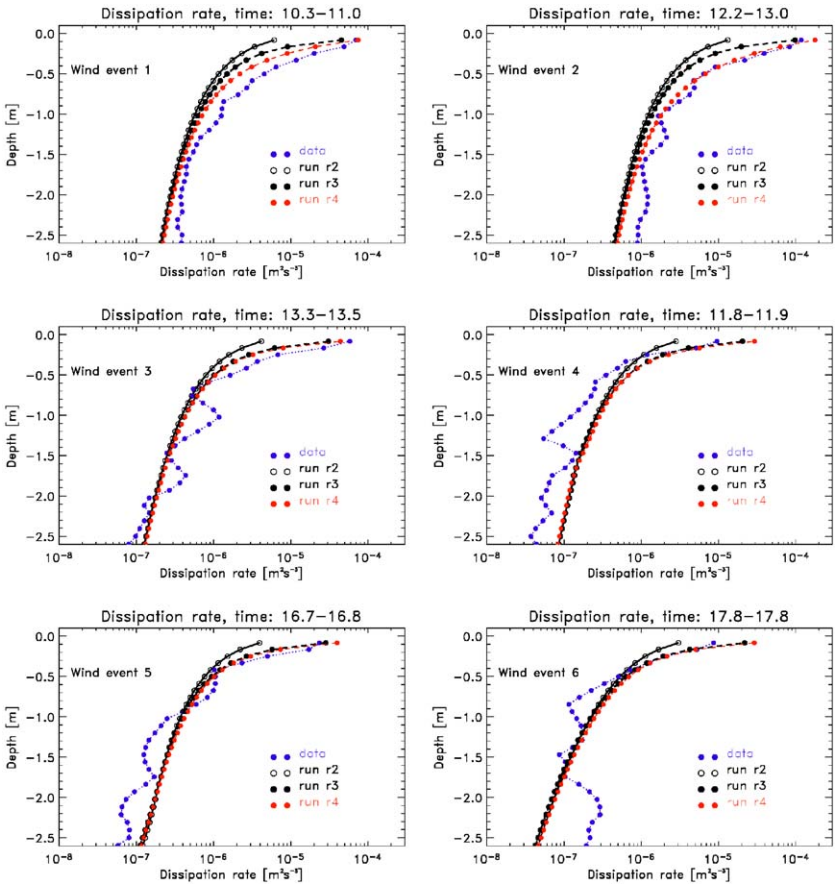

Fig. 8. Near surface profiles of dissipation rate for the selected 6 different wind events. Shown are the results from the simulation without wave breaking (run r2—black circles), simulation with wave breaking (run r3—black dots), simulation with increased z_0 (run r4—red dots) and the observed data (blue dots).

run r4. The influence of this increased z_0 on the minor wind events is minimal. As a side effect, the influence of the different window length on the average of the measured data becomes evident from Fig. 8. The decreasing averaging time from event 1 and 2 (around 18 h) to event 3 and 4 (around 3 h) and down to finally event 5 and 6 (around 1 h) leads to a much higher variability in the depth range below 1 m. Further it is demonstrated that already at such rather low wind speeds a clear signal from sporadic breaking events is evident.

In the depth range above about 1 to 0.5 m the simulated values from run r3 as well as the measured data deviate from the classical LOW slope of z^{-1}, which is represented by the open circles from run r2. The slope of ε in the uppermost 1 m was calculated using a least square fit for the decadal logarithm of ε with depth. The respective values found for the wind events are given in Table 6. Of course the unmodified k–ε model (run r2) leads to the expected slope of about z^{-1}. The improved model, including wave-breaking (run r3), provides near surface slopes of around $z^{-1.7}$, where as the measured longer wind events have a slope of about $z^{-1.9}$. The correlation coefficient is in all investigated cases around 0.99 (not shown). The depth of the WASL is likely to be depending on the wind speed and wave height. The depth of significantly increased ε is 1.3 m, 1.5 m and 0.6 m for wind event 1, 2 and 3, respectively (Fig. 8). This could be explained to be either about $3 \times H_S$ or could be calculated from a product of wind speed and wave height (to be scaled in order to get the correct dimension), but we have not enough points for an extended analysis.

Table 6
Table of mean slope of dissipation rate logarithm versus depth in the uppermost meter for the 6 identified wind events

Event	Run r2	Run r3	Run r4	Data
1	−0.97	−1.69	−1.94	−1.85
2	−0.99	−1.71	−1.96	−1.83
3	−0.97	−1.69	−1.83	−2.07
4	−0.96	−1.68	−1.85	−1.81
5	−0.97	−1.69	−1.79	−1.76
6	−1.06	−1.79	−1.87	−1.97

The slopes for the unmodified k–ε model are found under run r2, the results from the run r3 are with wave breaking parameterisation, results from run r4 are with wave breaking parameterisation using an increased surface roughness length and the measurements are under 'data'.

In the case of the two major wind events the measured uppermost ε value could fall in the depth of the wave-turbulent sublayer and would therefore scale different. There is indeed some indication that the measured uppermost ε does not continue the slope of the deeper values.

In case of the major wind events 1 and 2 we find also in the depth range below 1.5 m slightly increased dissipation rates. This is likely to be caused by higher order transport processes, which are not parameterised in the second order k–ε scheme. Only a model which also considers the third-order moments, like that described in Canuto et al. (1994) could be capable of reproducing such features. This finding is consistent with recent observations within Langmuir convergence zones, where vertical displacement of turbulence or vortex stretching result in slightly enhanced dissipation (Thorpe et al., 2003).

5. Discussion

5.1. General features of the simulations

In early March, the temperature stratification was very weak and temporal changes were dominated by advection of lateral inhomogeneities. It is clearly beyond the scope of the present paper to perform a 3D simulation on the investigated lake. Therefore the applied relaxation of the simulated temperature field to the measured temperatures represents a compromise between the sufficient accurate reproduction of the experimental data and the required effort. Only after applying relaxation of temperature (run r2) the simulated dissipation rate showed a similar dynamics as the measured, see Fig. 6. Moreover, during most of the time the unmodified k–ε model, especially near the surface (within the uppermost 1 m) underestimates the dissipation rates by up to one order of magnitude, see Fig. 7. Considering the prevailing light to moderate wind conditions which peak at 8 m s^{-1} at the profiler site, this might

come as a surprise. Through visual observations we considered first occurrence of white caps as an indication for wave breaking, which already started at around $3\,\mathrm{m\,s^{-1}}$. Using the wave breaking parameterisation as proposed by Craig and Banner (1994) and incorporated in the k–ε model by Burchard (2001b) certainly improved the simulation, as can be seen in Fig. 7. We however, found that the near surface ε values are still underestimated, especially in the case of the major wind events, but sometimes even during periods of low wind speeds.

5.2. Scaling of near surface dissipation rate

Applying appropriate scaling, near surface dissipation rates under breaking waves should collapse almost into one curve, see Terray et al. (1999). In the non-breaking case the near surface dissipation rate is usually made non-dimensional by applying the factor $1/(u_*^3/z_0)$ according to the LOW Lombardo and Gregg (1989), whereas the non-dimensional depth $\tilde{z}$ will become $(z_0 - z)/z_0$. Here we are using a surface roughness length calculated according to the Charnok formula, see Eq. (6). When wave-breaking is important the depth will be scaled by the significant wave height H_S instead, so that $\tilde{z} = (z_0 - z)/H_S$. The non-dimensional dissipation rate $\tilde{\varepsilon}$ will be defined as $\varepsilon/(c_w u_*^3/H_S)$, with $c_w = 100$ for all considered wind events. We can use a constant wave breaking parameter c_w, as the increasing probability of wave breaking with increasing wind speed is indirectly already accounted for by u_*^3 in the scaling law.

In Fig. 9 data and model results from this study are compared to published observations in the WASL by Terray et al. (1999), Drennan et al. (1996) and Anis and Moum (1995). The slope in our data is about -2.6 and therefore slightly lower than that from the other measurements. The applied scaling works for most of the data from events 1, 2 and 3 rather well, as the points fall practically on one line. An exception is the uppermost point for both major events, which does not follow that line. There is some speculation about the existence of a thin wave-turbulent layer of constant ε with thickness z_0 directly at the surface (Benilov and Ly, 2002; Burchard, 2001b).

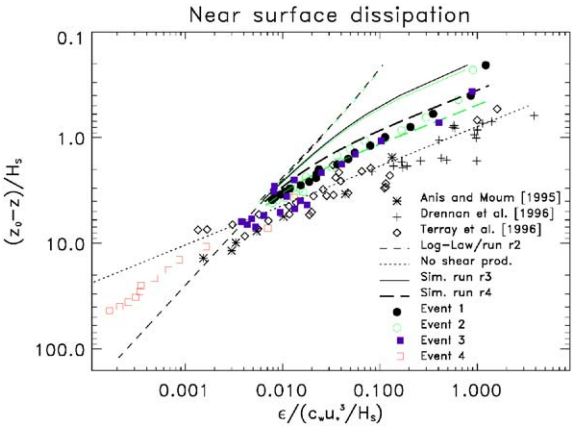

Fig. 9. Non-dimensional plot of observations and simulations of dissipation rate in the WASL. All observations are normalised by the surface TKE flux ($C_w u_*^2$) and the significant wave height H_S. The simulations of run r2 (short dashed lines) coincide with the classical LOW. The pure wave breaking case (no shear production) is shown by the dotted line. Simulations with wave breaking (run r3) are represented by the full lines, whereas the simulation with increased surface roughness length (run r4) is displayed by the longer dashed line. Experimental data are represented by the different symbols and colours. Black lines represent event 1 and green lines event 2.

This uppermost layer is directly mixed by wave breaking and turbulence production by the mean shear flow can be neglected. Therefore it will be relatively shear-free and this will result in a constant dissipation rate in that layer. This is further supported by the existence of this point, which appears to be scaled too small. For weaker wind and waves such a near surface outlier is not existing, a fact which is further supporting this speculation. The three sets of near surface dissipation rates from the literature, were scaled by Terray et al. (1999) using the significant wave height H_S. The ratio of z_0/H_S for these data is 0.85. Using z_0 values derived from the Charnok (1955) formula (Eq. (6)) as for run r2 we find z_0/H_S ratios of 0.012 and 0.022 for events 1 and 2, respectively. With such a low ratio the model underestimates the measured data. By far better is $10 \times z_0/H_S$, the ratio used for run r4, being 0.12 and 0.22 for events 1 and 2. Therefore, in accordance with Gemmrich and Farmer (1999), we would reject the assumption of a fixed z_0/H_S

ratio as done by Terray et al. (1999) and in this context their value of 0.85 seems far too large.

5.3. Surface roughness length

The determination of an appropriate surface roughness length seems to be the major problem for applying the new theory, as this input parameter must be provided a priori (from the measurements). Several authors (see Craig and Banner (1994), Terray et al. (1996), Drennan et al. (1996), Gemmrich and Farmer (1999)) had proposed that the relevant length scale at the surface in the case of wave-breaking will not be the surface roughness length of a classical LOW. Terray et al. (1996) and Drennan et al. (1996) proposed the significant wave height as the relevant length scale, but this was contradicted by Gemmrich and Farmer (1999).

We investigated the influence of different chosen z_0 on the simulations, especially on the fit in the WASL. When using GOTM, the simplest implementation is to change the coefficient α of the Charnok (1955) formula. Instead of the standard $\alpha = 1400$ (Craig and Banner, 1994) we tested values of 5600, 14,000 and 56,000, see also Stacey (1999). Then the resulting maximal z_0 for a wind speed of $5\,\mathrm{m\,s^{-1}}$ will be about 0.02, 0.05 and 0.2 m, respectively instead of 0.005 m for the standard value. Only when using $\alpha = 14,000$ the simulations agree rather well with the observations. The value of 5600 gives similar results as run r3 using the standard value and the largest value (56,000) leads to an unrealistic overestimation of the near surface dissipation. Enhanced dissipation rates extend to much greater depth then observed ones. Therefore we must conclude that at least for such small wind speeds as persisted during our experiment z_0 is larger than usually assumed, but still much smaller than the significant wave height H_S. This finding seems to contradict Terray et al. (1996), as they found that an appropriate z_0 would be in the order of H_S (Terray et al., 1996; Drennan et al., 1996; Craig, 1996; Stacey, 1999). Field measurements by Gemmrich and Farmer (1999) showed a much smaller z_0 and a different relation between significant wave height and surface roughness length. Gemmrich and Farmer (1999) found a z_0 of about 0.2 m for wind speeds of $U_{10} = 15\,\mathrm{m\,s^{-1}}$. Applying this increased coefficient in the Charnok formulation (Eq. (9)), would result in $z_0 \approx 0.165$ m for a wind speed of $15\,\mathrm{m\,s^{-1}}$. A wind speed of $U_{10} = 25\,\mathrm{m\,s^{-1}}$ would give a z_0 of 0.29 m. Therefore our results support the view of a smaller surface roughness length, whilst still larger than the conventionally assumed, would be defined in the following way:

$$z_0^{\mathrm{new}} = 14000\,u_*^2/g. \tag{9}$$

The uppermost point from the wind events 1 and 2 fall outside the applied scaling, see Fig. 9. This is indicative of the proposed layer of constant dissipation rate, as these values are representative for a depth of 0.075 m and therefore fall within in the depth range of the postulated breaking zone as found by Terray et al. (1996) $z_b \approx 0.6H_S$. The next deeper value at about 0.015 m depth would still fall within this depth range, but in our data it follows the proposed scaling with wind and wave forcing. Therefore this would also seem to support the view of a much shallower breaking zone in the order of z_0 only. The transition to the classical wall layer seems to appear at about a depth of 2–3 times the significant wave height.

5.4. TKE budget

An interesting question of relevance to the current analysis is, what are the contributions to the TKE production from shear, buoyancy and wave breaking during the identified wind events? Therefore we integrated dissipation rate, shear production P_S and buoyancy production P_B over the uppermost meter for the 6 identified wind events. The first obvious result is, that the contribution from buoyancy production P_B is negligible, as can be seen from the results presented in Table 7. We therefore do not consider further buoyancy production in this discussion. For run r2 the TKE production is not shown, as the unmodified k–ε model is based on the balance between TKE production and its dissipation, and therefore the respective values will be nearly identical to the dissipation rates. Simulated ε increased in run r3 by a factor of 2.5 compared to run r2, whereas P_S increased by a factor of 2.

Table 7
Table of depth integrated dissipation rate, shear production P_S and buoyancy production P_B of the uppermost meter for the 6 identified wind events

Event	ε (r2)	ε (r3)	P_S (r3)	P_B (r3)	ε (r4)	P_S (r4)	ε (data)
1	1.4	3.5	2.8	2.7e−3	6.4	1.3	11.4
2	3.0	7.6	6.1	7.3e−3	18.1	1.9	19.7
3	0.9	2.4	1.9	5.1e−3	3.0	1.3	5.9
4	0.6	1.6	1.2	1.2e−3	2.0	0.8	1.1
5	0.9	2.2	1.8	−7.0e−3	2.8	1.2	3.5
6	0.7	1.6	1.3	−2.2e−3	1.9	1.0	1.2

Results are shown from run r2 without wave breaking, run r3 with wave breaking parameterisation and from run r4 with increased roughness length z_0. The measured ε is found under 'data'. The units for all quantities is $10^{-3}\,\mathrm{W\,m^{-2}}$.

For run r3 shear production P_S is for all wind events about 80% of the respective dissipation rate. The simulated ε is again increased for run r4, now by a varying factor between 3 to 6 compared to run r2. The opposite effect is observed for P_S, which is now smaller than the values for run r3 and in the case of wind event 2 even smaller than that from run r2. This is related to the fact, that in this case TKE production in the near surface zone is mainly caused by wave breaking instead of shear production. The event 2, which had the strongest wind seems to be best simulated, as ε from run r4 and from the data agree rather well. In the case of the other two events with larger waves (1,3) the measured dissipation exceeds the simulated dissipation by approximately a factor of 2. Only in the case of the minor wind events 4 and 6, simulated dissipation is larger than the measured one. From these results it is obvious that near surface ε will be only simulated in the correct order of magnitude, when the TKE production due to breaking waves is taken into account.

We would like to further quantify the contributions to TKE production from the energy of breaking waves by using a simple linear model and from Stokes drift in order to estimate the importance of these processes. The linear model assumes that the rate of TKE production due to breaking waves P_{wave} [$\mathrm{W\,m^{-2}}$] is proportional to the wave energy content E_W [$\mathrm{J\,m^{-2}}$] multiplied by some inverse dissipation time scale of the wave energy (Longuet-Higgins, 1969):

$$P_{\mathrm{wave}} = 1600 C_D^{3/2} \frac{\rho_{\mathrm{Air}}}{\rho} f_p E_W, \tag{10}$$

where f_p is the peak frequency from Table 4. The resulting values from this linear model P_{wave} (Table 8) are always much smaller than the measured dissipation rate. For event 1 P_{wave} exceeds the simulated ε from run r3, but is lower than that from run r4. For the other two events with waves 2 and 3 this linear estimate is below ε from run r3. Therefore it is evident, that the linear wave breaking model alone cannot explain the measured near surface ε.

A different estimation for the surface flux of TKE due to breaking waves was proposed in Terray et al. (1996) and in Gemmrich and Farmer (1999)

$$P_{\mathrm{breaking}} = \overline{c_P} \rho u_*^2, \tag{11}$$

where u_* is the friction velocity in water and $\overline{c_P}$ is the effective phase speed of waves acquiring energy from the wind (Gemmrich et al., 1994). Using $\overline{c_P} \approx 0.1 c_P$ (Terray et al., 1996, Table 4) we will get values between 10 to $29 \times 10^{-3}\,\mathrm{W\,m^{-2}}$, see Table 8. These estimates exceed all other estimates and the measured turbulent dissipation rates. For the events 1, 2 and 3 P_{breaking} is between 20 and 70% above the measured ε, but they are in the same order of magnitude. Taking into account that the waves at lake Neuchâtel are young waves, then $\overline{c_P}$ should be even larger, which would result in even larger estimates. Eq. (11) assumes that there is no wave energy flux divergence, this likely

Table 8
Estimated TKE production due to wave breaking from the linear model and according to Eq. (11) are found under P_{wave} and P_{breaking}, respectively

Event	$\varepsilon - P_S$ (r4)	P_{wave}	P_{breaking}	P_{Stokes}
1	5.1	4.7	14	2.9
2	16.3	2.4	29	2.5
3	1.7	1.6	10	0.7
4	1.2	0.02	11	0.01
5	1.6	0.003	9	0.001

Production because of interaction between Stokes drift and Langmuir circulation is under P_{Stokes}. The units for all quantities is $10^{-3}\,\mathrm{W\,m^{-2}}$.

is not to be the case for young waves and therefore Eq. (11) overestimates the surface TKE flux in case of young waves.

The interaction of the vortex force associated with the Stokes drift u_s (see Stokes, 1847) and the mean current shear could be another potential source of TKE production (Skyllingstad and Denbo, 1995). This interaction can generate Langmuir circulations, that could potentially be a dominant mixing process in the SML. The production P_{Stokes} is then defined by

$$P_{\text{Stokes}} = \tau u_S \tag{12}$$

with u_S as defined in Eq. (8). Because of the exponential decay with depth of the Stokes drift, this related production will be confined to thin near surface layer, which scales with the inverse of the wavenumber k. In Table 8 it can be seen, that in the case of existing waves the related TKE production P_{Stokes} is of similar importance as the shear production or the production due to wave breaking estimated from the linear model. The contribution from wave breaking as simulated by the k–ε model is given in column 2 of Table 8 ($\varepsilon - P_S$). For events 1 and 3 this is similar to P_{wave}, but for event 2 it is a factor of 7 larger. Considering that this is opposite to the ε simulation, it seems that TKE production due to wave breaking is not well quantified yet.

It can be concluded that in the case of wind speeds above $3\,\text{m}\,\text{s}^{-1}$, but without corresponding wave development all energy estimates only based on wave parameters seem to fail. If similar wind speeds are accompanied by waves with significant wave heights of above 20 cm these equations give some first order approximation of the TKE production due to breaking waves, but linear model and Stokes drift underestimate, whereas Eq. (11) overestimates TKE production.

5.5. Intermittency

Wave breaking is a very intermittent process, therefore also the related turbulence levels are inferred to be intermittent. Phillips (1985) showed theoretically that breaking frequency and whitecap coverage should be proportional to u_*^3. It is probable that the measured mean turbulence level is orders of magnitude smaller than the level which occurred directly after a breaking event. Rapp and Melville (1990) estimated the temporal decay of dissipation rate ε beneath breaking laboratory waves, and found that $\varepsilon \propto t^{-5/2}$. Gemmrich (2000) states that for timescales comparable to the period of breaking waves, advection due to Langmuir circulation can be neglected. The time between successive breaking events at wind speeds between 3 and $6\,\text{m}\,\text{s}^{-1}$ is O(600 s),

The duration of breaking events is in the order of 0.5 to 3 s (see Gemmrich, 2000; Eifler and Donlon, 2001).

Considering this low breaking frequency, the short duration of the breaking events and the fast decay time of dissipation after the breaking event, we must ask ourselves, can we measure enhanced near surface dissipation rates due to wave breaking using vertical profiler snap shots?

Following Baker and Gibson (1987) we can estimate the intermittency factor of the measured dissipation rate as $\sigma^2_{\ln(\varepsilon)}$, which is the sample variance of the natural logarithm of ε. For the major wind events these intermittency factors fall in the range between 1.6 and 2.0 for the depth bins in the uppermost metre. Further down the water column they decrease and approach 1.0 at about 5 m depth. These values above 1.0 point to an enhanced intermittency, likely due to breaking events, but they are nevertheless much smaller than values (above 3.0) cited in Baker and Gibson (1987) for the thermocline or the equatorial undercurrent. Therefore the estimated mean values can be considered as representative.

The fact that we found enhanced near surface dissipation, could be explained by two possible factors, the first is that the decay time is much longer than usually assumed or the second being that we do not measure breaking events, but enhanced turbulence due to the interaction of the vortex force associated with surface waves and the mean current shear. Gemmrich (2000) concludes from his measurements that the decay time of breaking events is very short (less than 20–30 s), which would point to the second option. The only moderately increased intermittency factor found in the WASL also supports that short wave breaking events could only play a minor role for the

increased turbulence levels found. On the other hand the energy budget (Section 5.4) gave far too small values for the TKE production due to these nonlinear processes. Therefore we are not able to exclude one or the other possibility with certainty.

6. Summary and conclusions

Two major questions were examined in this paper, the first being, do we measure enhanced dissipation at the surface for wind speeds below $8\,m\,s^{-1}$ using a vertical profiler and the second can we simulate this wave affected surface layer (WASL) with current days turbulence models.

As has been shown in the previous sections, we find a layer of increased turbulence compared to the *law-of-the-wall* near the surface. Therefore the first question is answered positively, with vertical profiling instruments the enhanced turbulence in the WASL can be measured successfully. The profiling method is especially beneficial for completely assessing the topmost 1 m layer. We found the near surface slope of ε to be ≈ -2.0 in the case of wind speeds above $4\,m\,s^{-1}$. Further our high resolution near surface measurements of dissipation rate show already at wind speeds above about $2\,m\,s^{-1}$ clear evidence of a wave affected layer with increased ε compared to the classical *law-of-the-wall*, having a thickness between 0.1 and 1.2 m. In terms of the significant wave height H_S this wave affected layer reached to a depth of about 2 to $3 \times H_S$. This indeed provokes an additional question, of whether really only wave breaking could be the cause of this enhanced dissipation, or would there be other processes of importance, as the interaction of the mean current shear with the vortex force resulting form the Stokes drift. Considering that we found enhanced dissipation at rather low speeds, where breaking events are unlikely to occur gives some evidence to the assumption that these enhanced ε are not only caused by wave breaking. This question cannot be answered definitely in the frame of the present work, but should be addressed with specific measurement setups.

The other major issue addressed in the present manuscript was, to test if this wave affected layer can be reproduced by current day turbulence models. Here we have demonstrated that TKE dissipation rates in the near surface region were realistically simulated using the ID k–ε turbulence closure (GOTM), when the effects of wave breaking on turbulence production are considered. This is true with both, with regard to the magnitude of the near surface dissipation, as well as the depth range of the increased ε and the exponential decay of ε away from the surface, showing a power law of about $z^{-1.9}$. Using non-dimensional dissipation and depth, the power law will be $\tilde{z}^{-2.5}$.

Obviously one of the major problems for successful simulating near surface turbulence is not directly related to the modelling itself, but how to find proper values for the surface roughness length, as the most critical model input parameter. Only when increasing the surface roughness length z_0 calculated from the Charnok formula by a factor of 10, the dissipation rate in the wave affected layer could be realistically simulated. Therefore it seems also that we are still lacking some basic physical understanding of the meaning of the roughness length in the case of breaking waves. We could not confirm that z_0 would scale with the significant wave height as assumed by Drennan et al. (1996). The best fit to our data, if scaled to a wind of $15\,m\,s^{-1}$, would result in z_0 values of similar magnitude (about 20% smaller) as reported by Gemmrich and Farmer (1999).

In summary our results clearly support the view of a smaller surface roughness length as proposed by Craig and Banner (1994), Drennan et al. (1996) or Stacey (1999), but still much larger than the ones assumed conventionally. Care should be taken that the wave affected layer showing increased dissipation rates in the depth range of order of 1 to $3 \times H_S$ is not confused with the surface roughness length. The measurements further indicate, that an assumed wave breaking zone having a constant dissipation rate would exist only in the depth range of the increased z_0 (1–20 cm).

Future work should be directed to measurements, that would allow to separate shear-generated turbulence production from wave-breaking-generated turbulence, in order to clarify the contributions from each part to the near surface

production. In order to get a more complete picture of near-surface turbulence, different types of measurements should be combined (e.g. fixed and wave following sensors). But most importantly work must be carried out to determine the surface roughness length (or surface mixing length as proposed by Gemmrich and Farmer, 1999) as a function of wind and wave parameters. This analysis would also clarify if really a layer of constant ε exists near to the surface.

Acknowledgements

Performing this extensive measurement campaign was only possible with the help of several colleagues from the Environmental Physics department at EAWAG and the Inland and Marine Waters Unit of JRC. Thanks to all of them, but especially to Otti Kocsis, Michael Schurter, Ulisse Devisioni, Bjarke Rasmussen and Alexander Pufahl. Ute Stips volunteered to reprocess the shear data and made the quality control of the dissipation rate data. Mark Dowell helped to polish our English. The constructive comments of Alastair Jenkins and an anonymous reviewer improved the paper further.

Appendix A

Here, it is briefly demonstrated how some of the empirical parameters for the extended k–ε model are calculated. This extends the algebra contained in Burchard (2001a) which was shown for the standard k–ε model with constant c_μ, only. Here, the stability functions of Canuto et al. (2001) with shear-dependence are used. The stability function for LOW conditions is calculated by means of $P+B=\varepsilon$ which is equivalent to

$$c_\mu(\alpha_M,\alpha_N)\alpha_M - c'_\mu(\alpha_M,\alpha_N)\alpha_N = 1 \qquad (13)$$

with the stability functions c_μ and c'_μ for momentum and tracers, respectively, the shear and buoyancy parameters, $\alpha_M = M^2k^2/\varepsilon^2$ and $\alpha_N = N^2k^2/\varepsilon^2$, respectively, and the shear squared, $M^2=(\partial_z u)^2+(\partial_z v)^2$ and the Brunt-Väisälä frequency squared, $N^2=-(g/\rho_0)\partial_z\rho$. The numerical solution of the implicit function for $\alpha_N=0$ is $c_\mu=0.07715$. For shear-free turbulence with $P_S/\varepsilon=0$ and thus $\alpha_M=\alpha_N=0$ we computed directly from the definition of the Canuto et al. (2001) stability functions that $c_\mu=0.107$. With the other parameters given in Table 1, Eqs. (14), (16) and (17) in Burchard (2001a) compute directly $m=2.238$, $\sigma_{\varepsilon,\mathrm{LOW}}=1.2$ and $\sigma_{\varepsilon,\mathrm{WASL}}=2.012$.

References

Agrawal, Y.C., Terray, E.A., Donelan, M.A., Hwang, P.A., Williams III, A.J., Drennan, W.M., Kahma, K.K., Kitaigorodskii, S.A., 1992. Enhanced dissipation of kinetic energy beneath surface waves. Nature 359, 219–220.

Anis, A., Moum, J.N., 1992. The superadiabatic surface layer of the ocean during convection. Journal of Physical Oceanography 22, 1221–1227.

Anis, A., Moum, J.N., 1995. Surface wave-turbulence interactions: scaling $\varepsilon(z)$ near the sea surface. Journal of Physical Oceanography 25, 2025–2045.

Baker, M.A., Gibson, C.H., 1987. Sampling turbulence in the stratified ocean: statistical consequences of strong intermittency. Journal of Physical Oceanography 17, 1817–1836.

Benilov, A.Y., Ly, L.N., 2002. Modelling of surface waves breaking effects in the ocean upper layer. Mathematical and Computer Modelling 35, 191–213.

Bishop, C.T., Donelan, M.A., 1987. Measuring waves with pressure transducers. Coastal Engineering 11, 309–328.

Burchard, H., 2001a. On the q^2l equation by Mellor and Yamada [1982]. Journal of Physical Oceanography 31, 1377–1387.

Burchard, H., 2001b. Simulating the wave-enhanced layer under breaking surface waves with two-equation turbulence models. Journal of Physical Oceanography 31, 3133–3145.

Burchard, H., 2002. Applied Turbulence Modelling in Marine Waters. Lecture Notes in Earth Sciences, vol. 100. Springer, Berlin, Heidelberg, New York.

Burchard, H., Baumert, H., 1995. On the performance of a mixed-layer model based on the k–ε turbulence closure. Journal of Geophysical Research 100, 8523–8540.

Burchard, H., Bolding, K., 2002. GETM, a general estuarine transport model. Technical Report EUR 20253, European Commission, Ispra.

Burchard, H., Deleersnijder, E., 2001. Stability of algebraic non-equilibrium second-order closure models. Ocean Modelling 3, 33–50.

Burchard, H., Bolding, K., Ruiz-Villarreal, M., 1999. GOTM-a general ocean turbulence model. Theory, applications and test cases. Technical Report EUR 18745 EN, European Commission.

Burchard, H., Stips, A., Eifler, W., Bolding, K., Villarreal, M.R., 2000. Numerical simulation of dissipation measurements in non-stratified and strongly stratified estuaries. In: Yanagi, T. (Ed.), Interactions Between Estuaries, Coastal

Seas and Shelf Seas. Terra Scientific Publishing, Tokyo, pp. 1–18.

Businger, J.A., Wyngaard, J.C., Izumi, Y., Bradley, E.F., 1971. Flux profile relationships in the atmospheric surface layer. Journal of Atmospheric Sciences 28, 181–189.

Canuto, V.M., Minotti, F., Ronchi, C., Ypma, R.H., Zeman, O., 1994. Second-order closure PBL model with new third-order moments: comparison with LES data. Journal of Atmospheric Sciences 51, 1605–1618.

Canuto, V.M., Howard, A., Cheng, Y., Dubovikov, M.S., 2001. Ocean turbulence. Part I: one-point closure model—momentum and heat vertical diffusivities. Journal of Physical Oceanography 31, 1413–1426.

Charnok, H., 1955. Wind stress on a water surface. Quarterly Journal of the Royal Meteorological Society 81, 639–640.

Craig, P.D., 1996. Velocity profiles and surface roughness under breaking waves. Journal of Geophysical Research 101, 1265–1277.

Craig, P.D., Banner, M.L., 1994. Modelling wave-enhanced turbulence in the ocean surface layer. Journal of Physical Oceanography 24, 2546–2559.

Dillon, T.M., Richman, J.G., Hansen, C.G., Pearson, M.D., 1981. Near-surface turbulence measurements in a lake. Nature 290, 390–392.

Donelan, M.A., 1998. Air-water exchange processes. In: Imberger, J. (Ed.), Physical Processes in Lakes and Oceans. Coastal and Estuarine Studies, vol. 54. American Geophysical Union, Washington, DC, pp. 19–36.

Drennan, W.M., Donelan, M.A., Terray, E.A., Katsaros, K.B., 1996. Oceanic turbulence dissipation rate measurements in SWADE. Journal of Physical Oceanography 26, 808–815.

Eifler, W., Donlon, C.J., 2001. Modeling the thermal surface signature of breaking waves. Journal of Geophysical Research 106, 27163–27185.

Gemmrich, J.R., 2000. Temperature anomalies beneath breaking waves and the decay of wave-induced turbulence. Journal of Geophysical Research 105, 8727–8736.

Gemmrich, J.R., Farmer, D.M., 1999. Near-surface turbulence and thermal structure in a wind-driven sea. Journal of Physical Oceanography 29, 480–499.

Gemmrich, J.R., Farmer, D.M., 2004. Near-surface turbulence in the presence of breaking waves. Journal of Physical Oceanography, (in print).

Gemmrich, J.R., Mudge, T.D., Polonichko, V.D., 1994. On the energy input from wind to surface waves. Journal of Physical Oceanography 24, 2413–2417.

Gibson, C.H., 1982. Alternative interpretations for microstructure patches in the thermocline. Journal of Physical Oceanography 12, 374–383.

Greenan, B.J.W., Oakey, N.S., Dobson, F.W., 2001. Estimates of dissipation in the ocean mixed layer using a quasi-horizontal microstructure profiler. Journal of Physical Oceanography 31, 992–1004.

Henderson-Sellers, B., 1986. Calculating the surface energy balance for lake and reservoir modeling: a review. Reviews of Geophysics 24, 625–649.

Janssen, P.A.E.M., 1989. Wave-induced stress and the drag of air flow over sea waves. Journal of Physical Oceanography 19, 745–772.

Jenkins, A.D., 1987. Wind and wave induced currents in a rotating sea with depth-varying eddy viscosity. Journal of Physical Oceanography 17, 938–952.

Jenkins, A.D., 1989. The use of a wave prediction model for driving a near-surface current model. Deutsche Hydrographische Zeitschrift 42, 133–149.

Jenkins, A.D., 1992. A quasi-linear eddy-viscosity model for the flux of energy and momentum to wind waves using conservation-law equations in a curvilinear coordinate system. Journal of Physical Oceanography 22, 843–858.

Jenkins, A.D., 1993. A simplified quasi-linear model for wave generation and air-sea momentum flux. Journal of Physical Oceanography 23, 2001–2018.

Kantha, L.H., Clayson, C.A., 2004. On the effect of surface gravity waves on mixing in the oceanic mixed layer. Ocean Modelling 6, 101–124.

Kitaigorodskii, S.A., Donelan, M.A., Lumley, J.L., Terray, E.A., 1983. Wave turbulence interactions in the upper ocean. Part II: statistical characteristics of wave and turbulent components of the random velocity field in the marine surface layer. Journal of Physical Oceanography 13, 1988–1999.

Kocsis, O., Prandke, H., Stips, A., Simon, A., Wiiest, A., 1999. Comparison of dissipation of turbulent kinetic energy determined from shear and temperature microstructure. Journal of Marine Systems 21, 67–84.

Lass, H.U., Prandke, H., 2003. A study on the turbulent mixed layer in the Baltic Sea. In: Chmielewski, F.M., Foken, T. (Eds.), Beiträge zur Klimaund Meeresforschung. Bayreuth, Berlin, pp. 159–168.

Lombardo, C.P., Gregg, M.C., 1989. Similarity scaling of viscous and thermal dissipation in a convecting surface boundary layer. Journal of Geophysical Research 94, 6273–6284.

Longuet-Higgins, M.S., 1953. Mass transport in water waves. Philosophical Transactions of the Royal Society Series A 245, 535–581.

Longuet-Higgins, M.S., 1969. On wave breaking and the equilibrium range of wind-generated waves. Proceedings of the Royal Society of London Series A 310, 151–159.

Lorke, A., Wüest, A., 2002. Probability density of displacement and overturning length scales under diverse stratification. Journal of Geophysical Research 107, 3214–3225.

Mellor, G.L., Yamada, T., 1974. A hierarchy of turbulence closure models for planetary boundary layers. Journal of Atmospheric Sciences 31, 1791–1806.

Mellor, G.L., Yamada, T., 1982. Development of a turbulence closure model for geophysical fluid problems. Reviews of Geophysics 20, 851–875.

Monin, A.S., Obukhov, A.M., 1954. Basic laws of turbulent mixing in the ground layer of the atmosphere. Translations Geophysics Institute, Akademiia Nauk SSSR, 24 (151), 163–187.

Moum, J.N., Lueck, R.G., 1985. Causes and implications of noise in oceanic dissipation measurements. Deep-Sea Research 32, 379–390.

Osborn, T.R., Farmer, D.M., Vagle, S., Thorpe, S.A., Cure, M., 1992. Measurements of bubble plumes and turbulence from a submarine. Atmosphere–Ocean 30, 419–440.

Phillips, O.M., 1985. Spectral and statistical properties of the equilibrium range in wind-generated gravity waves. Journal of Fluid Mechanics 156, 505–531.

Phillips, O.M., Posner, F.L., Hansen, J.P., 2001. High range resolution radar measurements of the speed distribution of breaking events in wind-generated ocean waves: surface impulse and wave energy dissipation rates. Journal of Physical Oceanography 31, 450–460.

Prandke, H., Stips, A., 1998. Test measurements with an operational microstructure-turbulence profiler: detection limit of dissipation rates. Aquatic Sciences 60, 191–209.

Rapp, R.J., Melville, W.K., 1990. Laboratory measurements of deep-water breaking waves. Philosophical Transactions of the Royal Society of London Series A 331, 731–800.

Rodi, W., 1980. Turbulence models and their application in hydraulics. Technical Report, Int. Assoc. for Hydraul. Res., Delft, The Netherlands.

Sander, J., Simon, A., Jonas, T., Wüest, A., 2000. Surface turbulence in natural waters: a comparison of large eddy simulations with microstructure observations. Journal of Geophysical Research 105, 1195–1207.

Simon, A., 1997. Turbulent mixing in the surface boundary layer of lakes. Ph.D. Thesis, Swiss Federal Institute of Technology, Zürich, Switzerland, Diss, ETH No. 12272.

Simpson, J.H., Burchard, H., Fisher, N.R., Rippeth, T.P., 2002. The semidiurnal cycle of dissipation in a ROFI: model-measurement comparisons. Continental Shelf Research 22, 1615–1628.

Skyllingstad, E.D., Denbo, D.W., 1995. An ocean large-eddy simulation of Langmuir circulations and convection in the surface mixed layer. Journal of Geophysical Research 100, 8501–8522.

Smith, S.D., 1988. Coefficients for sea surface wind stress, heat flux, and wind profiles as a function of wind speed and temperature. Journal of Geophysical Research 93, 15467–15472.

Soloviev, A.V., Lukas, R., 2003. Observation of wave-enhanced turbulence in the near-surface layer of the ocean during TOGA COARE. Deep-Sea Research I 50, 371–395.

Soloviev, A.V., Vershinsky, N.V., Bezverchnii, V.A., 1988. Small-scale turbulence measurements in the thin surface layer of the ocean. Deep-Sea Research 35, 1859–1874.

Stacey, M.W., 1999. Simulation of the wind-forced near-surface circulation in Knight Inlet: a parameterization of the roughness length. Journal of Physical Oceanography 29, 1363–1367.

Stips, A., Prandke, H., 2000. Recommended algorithm for dissipation rate calculation within PROVESS. Technical Report 1.00.116, European Commission, Joint Research Centre, Ispra, Italy.

Stips, A., Burchard, H., Bolding, K., Eifler, W., 2002. Modelling of convective turbulence with a two-equation k–ε turbulence closure scheme. Ocean Dynamics 52, 153–168.

Stokes, G.G., 1847. On the theory of oscillatory waves. Transactions of the Cambridge Philosophical Society 8, 441–455.

Terray, E.A., Donelan, M.A., Agrawal, Y.C., Drennan, W.M., Kahma, K.K., Williams III, A.J., Hwang, P.A., Kitaigorodskii, S.A., 1996. Estimates of kinetic energy dissipation under breaking waves. Journal of Physical Oceanography 26, 792–807.

Terray, E.A., Drennan, W.M., Donelan, M.A., 1999. The vertical structure of shear and dissipation in the ocean surface layer. In: Banner, M.L. (Ed.), The Wind-driven Air–Sea Interface—Electromagnetic and Acoustic Sensing, Wave Dynamics and Turbulent Fluxes. University of New South Wales, Sydney, pp. 239–245.

Thorpe, S.A., 1977. Turbulence and mixing in a Scottish loch. Philosophical Transactions of the Royal Society of London, Series A 286, 125–181.

Thorpe, S.A., Osborn, T.R., Jackson, J.F.E., Hall, A.J., Lueck, R.G., 2003. Measurements of turbulence in the upper-ocean mixing layer using autosub. Journal of Physical Oceanography 33, 122–145.

Umlauf, L., Burchard, H., 2003. A generic length-scale equation for geophysical turbulence models. Journal of Marine Research 61, 235–265.

Umlauf, L., Burchard, H., Bolding, K., 2005. General ocean turbulence model. Source code documentation. Technical Report, Baltic Sea Research Institute, Warnemünde, Germany (in print).

Zhang, K.Q., Chan, E.S., 2003. Modeling of the turbulence in the water column under breaking wind waves. Journal of Oceanography 59, 331–341.